KERNFORSCHUNGSZENTRUM

KARLSRUHE

April 1973 KFK 1770

Institut für Angewandte Kernphysik

A Study of the De-excitation of Primary Fission Fragments from the Neutron-induced Fission of U-235

Tasneem A. Khan, D. Hofmann, F. Horsch

GESELLSCHAFT
FÜR
KERNFORSCHUNG M.B.H.

KARLSRUHE

GESELLSCHAFT FÜR KERNFORSCHUNG M. B. H.
KARLSRUHE

KERNFORSCHUNGSZENTRUM KARLSRUHE

KFK 1770

Institut für Angewandte Kernphysik

A Study of the De-Excitation of Primary Fission Fragments from the Neutron-Induced Fission of U-235

Tasneem A. Khan[+], D. Hofmann[++] and F. Horsch

Gesellschaft für Kernforschung mbH, Karlsruhe

[+]Present address: Pakistan Atomic Energy Commission, PINSTECH, Nilore, Rawalpindi

[++]Inst. für Kernphysik, Universität Frankfurt/Main

Abstract

Two separate three-dimensional experiments have been performed in which the energies of coincident fragment pairs and gamma-rays or internal conversion electrons, emitted within $\approx$ 1.6 nsec after the thermal neutron induced fission of ^{235}U, were recorded event by event. The fragment kinetic energies were used for mass identification. The self consistency of the values of electron energy, gamma-ray energy and fragment charge, and its agreement with X-ray selection data, were used to identify the atomic number of the fragments. The analysis of the gamma ray and conversion electron spectra has resulted in the assignment of many transitions to new isotopes as well as improvement in or confirmation of many assignments from the ^{252}Cf spontaneous fission data. Limited information on the multipolarities of the transitions in even nuclei is presented. The relative yield of electrons per fragment indicates softness to deformation in mass region 100 - 110. Data are presented supporting the assignment of a 193 keV transition as the 2^+ to 0^+ transition in ^{98}Sr. An examination of the 2^+ level systematics of neighbouring even nuclei suggests a transition from vibrational to rotational behaviour in the light fragments between neutron numbers 58 and 60.

Zusammenfassung

Zwei Dreiparameterexperimente wurden durchgeführt, in denen einmal die Gammaenergien, das andere Mal die Energien der Konversionselektronen innerhalb $\approx$ 1.6 nsec nach der neutroneninduzierten Spaltung des ^{235}U gemessen wurden. Die Zuordnung zu spezifischen Spaltfragmenten geschah über die Methode der korrelierten Energiemessung. Die Selbstkonsistenz der Elektronenenergien, der Gammaenergien und der Ladungszahlen, und die gute Übereinstimmung mit Daten aus Röntgenquanten-Gamma-Koinzidenzmessungen, wurden als Grundlage der Zuordnung der Ordnungszahlen benutzt. Es war möglich, viele Übergänge neuen Isotopen zuzuordnen und mehrere Ergebnisse aus Untersuchungen an ^{252}Cf [s.f.] zu bestätigen oder zu verbessern. Aufgrund der gemessenen K/L-Verhältnisse konnte Information über die Multipolaritäten mehrerer niedrigliegender Übergänge in geraden Kernen gewonnen werden. Die relative Ausbeute der Elektronen pro Spaltprodukt weist auf eine Bereitschaft zur Deformation im Massenbereich 100 - 110 hin. Die gewonnenen Daten stützen die Interpretation einer 193 keV - Linie als $2^+ \rightarrow 0^+$-Übergang in ^{98}Sr. Der systematische Gang der 2^+ Niveauenergien durch benachbarte g-g-Kerne deutet auf einen Übergang vom Vibrations- zum Rotationsverhalten in den leichten Spaltfragmenten zwischen den Neutronenzahlen 58 bis 60 hin.

1. Introduction

There is an increasing interest in the study of nuclei far away from the stability line. Such studies help to explore the new regions of nuclear deformations and to extend nuclear theory to regions which have hitherto been inaccessible. Primary fission fragments, with their large excess of neutrons, 6 to 10 units [$\hbar$] of angular momentum and moderately high excitation energies, form a special class of nuclei far away from the stability line. Moreover they cover two very significant regions of nuclear deformation. The study of their nuclear properties is therefore of considerable interest.

Experimentally the study of the de-excitation of the primary fission fragments within the first few nanoseconds after fission is rather difficult, due to the fact that there is no way to study one isotope without interfering radiation from numerous others. However, with present-day techniques it is possible to measure the energies of the fission fragments, as well as the energy of any radiation emitted by the fragments, for individual fission events. Considerations of momentum and mass conservation then enable one to obtain the mass of the fragment giving rise to the radiation. Experiments of this type have been performed to study the gamma rays[1,2] and conversion electrons[3] from the fragments of ^{252}Cf[sf]. It was felt desirable to extend these measurements to thermal neutron induced fission firstly to investigate those nuclei whose yield in the spontaneous fission of ^{252}Cf is low and secondly to obtain more information on the mass region accessible to both ^{252}Cf[sf] and ^{235}U[n,f] and compare the results of the two fissioning systems.

The present work summarises the results of the investigations of the spectra of gamma rays[4,5] and internal conversion electrons[6] associated with intervals of fragment mass using the neutron induced fission of ^{235}U. Whereas the gamma-ray experiments explored the relatively higher energy transitions [> 150 keV] the electron measurements were mainly concerned with the large number of low energy transitions. It was attempted to obtain the electron spectra with high enough resolution to obtain the K/L ratios of the strongest transitions and thus assign multipolarities to them. By comparing the electron line energies with the energies of the corresponding gamma rays, assignments of the charge of the fragment was in many cases possible.

2. Experimental Procedures

2.1 GAMMA RAY MEASUREMENTS

A detailed description of the experimental procedure is given elsewhere[7]; therefore only the basic principles of the procedure will be outlined. The experimental set up was designed in such a way that the assignment of single gamma ray lines to specific fragments on the basis of the direction of the Doppler shift was possible. A schematic view of the experimental arrangement is shown in fig.1. A well collimated and filtered neutron beam from the FR2 reactor was made to strike a 50 $\mu g\ cm^{-2}$ target of ^{235}U on a 30 $\mu g\ cm^{-2}$ VYNS backing. The mass of the fragment giving rise to the radiation was determined from the kinetic energies of the fission fragments as measured by two Si surface barrier detectors. The gamma rays emitted by the fragments were detected by a 28 cc Ge[Li] detector which had a resolution of 3.5 keV for the 1332 keV gamma ray of ^{60}Co. A NaI[Tl] anti-Compton shield reduced the Compton distribution and the fast fission neutron induced lines in the gamma ray spectra. The gamma ray collimator was designed in such a way that the Ge[Li] detector could see both the fragments in flight, from their origin at the target to an average distance of about 1.6 cm. The actual fragment flight paths seen by the detector ranged between 1 to 2 cm. By this arrangement it was possible to assign a specific line to a particular member of each fragment pair by the sign of the observed Doppler shift in the gamma ray energy caused by the moving fragments.

The three analog pulse heights in each triple coincidence event were digitised and stored event by event in a 256 x 256 x 2048 channal matrix and processed via the Karlsruhe Multiple Input Data Acquisition system [MIDAS]. The masses of the fragments were calculated from the measured energies. The method used is outlined in the appendix. Final post neutron emission masses were calculated off line using experimental neutron numbers to correct for the emission of prompt neutrons. Gamma-ray spectra associated with fragment masses in 2 amu wide mass intervals were obtained by sorting the three parameter data. Each of these spectra was then analysed to give quantitative energies and intensities of individual transitions. Four typical examples of the mass sorted gamma ray spectra are shown in fig. 2.

2.2 ELECTRON MEASUREMENTS

The precise measurement of electron energies requires not only the elimination of any window for the electrons to penetrate that would seriously degrade their resolution, but also the mitigation of the doppler broadening of the electron lines by the moving fragments. The manner in which these problems were resolved may be seen in fig. 3. A well collimated neutron beam impinged on a target of ^{235}U. The energies of the fission fragments were measured by two silicon surface barrier detectors which were collimated to 20 mm in diameter and operated at - 50°C. The internal conversion electrons emitted by one of the fragments during the first 1.8 cm of its flight path were focussed on to an ion implanted detector by means of a doubly focusing magnetic field. The magnetic field steered the electrons round a lead shield which protected the detector from the intense prompt gamma ray background. The 200 mm^2 x 2 mm electron detector was operated at liquid nitrogen temperatures and had a resolution of about 3 keV in the region of interest.

The length of the fragment flight path was chosen to be as close as possible to the flight path of the fragments in the gamma ray experiment so that the results of the two experiments could be compared. However, unlike the gamma ray set up, electrons from only one of the fragments could arrive at the electron detector. The angles of emission of the electrons with respect to the fragment path were restricted to very nearly 90°. The serious losses of energy resolution due to the doppler broadening by the moving fragments were thus mitigated at the expense of a much lower count rate. However by using a target of thickness 100 $\mu g\ cm^{-2}$ on a 30 $\mu g\ cm^{-2}$ backing of VYNS and a neutron flux of 10^9 n cm^{-2} sec^{-1} a count rate of 20 events per minute was possible. Since only those electrons within a certain energy window were focussed on the electron detector for a particular value of the magnetic field, the field was made to sweep back and forth continuously throughout the experiment.

A block diagram of the electronics is shown in fig. 4. The pulses from the three detectors were amplified by low noise preamplifiers and routed to the three ADC's of the MIDAS system through linear and variable gain amplifiers. The three ADC's were gated by a timing system which required a threefold coincidence of events in the fission fragment and electron detectors. The coincidence resolving time was

80 nsec and any pile up of pulses in the fission detectors generated a veto signal in the gating circuit.

As the measurements were made over several months, digital stabilisation was used on all three detectors to avoid any possible gain shifts. The D.C. levels of the three detectors, as well as the gain of the electron detector were stabilised by monitoring precision pulsers. The gains of the fragment detectors were stabilised by monitoring the energies of the light fragment peaks. At the end of every 24 hours of measurement calibration checks were made for stability by sliding the built in calibration sources of ^{137}Cs and ^{57}Co under the electron detector and observing the positions of the 129 keV and 624 keV electron lines. A two parameter experiment to obtain the correlated energies of the two fission fragments was also performed at this time. This enabled one to obtain a set of calibration constants for the fragment detectors for each 24 hour period and to monitor the quality of these detectors continuously. The events accumulated daily in the two parameter experiments were summed over the entire period of measurements and used to obtain the mass yield curve for the neutron induced fission of ^{235}U. At the end of each reactor period a calibration of electron energy versus channel number was made by means of ^{133}Ba, ^{57}Co and ^{137}Cs sources, which gave a number of lines over the entire region of interest.

During the course of the measurements a total of 1 million events for the 3 parameter electron experiment and a similar number for the two parameter experiment were accumulated. Part of the three parameter data was accumulated during subsequent runs confined to the 200 to 350 keV region of electron energies. The data was processed by procedures similiar to those described for the gamma-ray experiment and electron spectra associated with fragment masses in 2 a.m.u. mass intervals were obtained. Two examples of such mass sorted spectra accumulated during the first half of the measurements are shown in fig. 5 and fig. 6. The former is from the light and the latter from the heavy fragment groups.

3. Results

3.1 GAMMA RAY MEASUREMENTS

In table 1 54 gamma-rays have been assigned to individual fragments. The masses were obtained by plotting the peak intensities as a function of mass. The

first moments of these distributions then identified the mass of the fission fragment and the widths established the mass resolution. The magnitude of the widths is determined by the dispersion introduced in prompt neutron emission and by the inherent energy resolution of the fission fragment detectors. In the present case the mass resolution ranged from 4 to 7 a.m.u. FWHM. Only those gamma transitions have been included in table 1 for which both Doppler shifted members were well enough resolved to be identified on the basis of a congruous intensity vs mass distribution. The absolute uncertainties in the mass determination are mainly due to systematic errors in the calibration procedure and the neutron corrections.

The most probable charges Z_p were taken from the tables of Wahl et al.[8] starting from the original non integral mass values derived. Due to the small width of the charge distribution for a given mass [$\approx$1.5 charge units FWHM] the true charge should generally lie within $\pm$ 1 unit of Z_p since only transitions in fragments with fairly high yield [> 0.5 %] are resolved in the present experiment. The gamma ray energies are the mean values of the Doppler pairs.

The error bars are based on both uncertainties in the determination of the peak positions and systematic errors. For fission fragments travelling in the direction of maximum detection efficiency, i.e. approximately towards the centre of the fragment detectors, the flight path viewed by the gamma detector was 16 mm. This corresponds to about 1.1 nsec for the light fragments and 1.7 nsec for the heavy fragments. Therefore the experimental intensity values represent the relative number of quanta emitted within these times after fission. A large number of transitions may be identified on the basis of the close agreement in energy, charge and mass assignment with those observed in fragments from the spontaneous fission of ^{252}Cf [1,2,9]. Other interpretations are based upon the systematics of $2^+ \rightarrow 0^+$ transitions in neighbouring even nuclei or upon close agreement of energy and mass assignment with [t,p][10] and beta decay data [13]. The interpretations are also supported by the results of the electron measurements as well as the fact that the intensities of transitions assigned as $2^+ \rightarrow 0^+$ in even-even nuclei in the present work follow the calculated independent yields of the isotopes, as discussed in subsect. 4.2.

Many of the low energy gamma rays observed could be related to conversion electron lines seen in the electron experiment. These lines are indicated by an asterisk before the line energy in table 1. Further information about these lines is given in the table 2 which summarises the results of the electron experiment.

3.2 ELECTRON MEASUREMENTS

A total of 131 lines have been analyzed in the electron spectra out of which 63 belong to the light fragment group and 68 to the heavy fragments. The masses of the fragments were determined from the centroid of a plot of electron peak intensities as a function of mass as discussed in the previous section. The energies of the electron lines were determined by a least square analysis of the electron spectra using the calibration methods outlined in subsect. 2.2. In calculating gamma ray transition energies from the conversion electron energies, account has to be taken of the increase in electron binding energies due to the high states of ionization of the fragments. This correction, which is nearly constant and about 0.9 keV over the range of elements produced in fission[3], has been made in the present data, and therefore the electron energies are compatible with gamma ray energies from stopped fission fragments. The electron energies in the present experiment are estimated to have an error of $\pm$ 1 keV.

In order to determine the charge of the fragments two procedures were adopted:

[1] The results of the present experiment were compared with the work of Hopkins et. al.[11,12] in which they have studied gamma rays in coincidence with X-rays from stopped fission fragments of ^{252}Cf. In their experiment the energies of a large number of low energy gamma rays is measured accurately and the coincident X-ray is used to give information regarding the charge of the fragment. The experiment restricts the possible origin of the gamma rays to a pair of complimentary fragments. In the present work, since we observe conversion electrons from only one of the two fragments and sort the spectra according to fragment mass, by a comparison of the results of the two experiments, it is possible to determine whether the electron [and gamma ray] line originated from the heavy or light fragment, and to assign a mass number to the fragment. The procedure was to obtain the K electron energies from the gamma rays using the binding energies of both

the fragments. By comparing the K line energies with the electron lines observed it was possible to determine not only which of the two fragments the electron line belonged to but also to ascertain that it was not from a neighbouring element. [2] As a further check on the above procedure and for those electron lines whose corresponding gamma rays were not observed in the work of Hopkins et. al., the binding energies of the elements around the most probable charge were used to calculate the corresponding gamma ray energies for the electron lines observed. The results were compared with the energies of gamma rays measured in the gamma ray experiment of the present work and the work on ^{252}Cf fission [1,2,9], and the element with the binding energy which gave the best fit was assigned.

In the atomic numbers assigned in the present work, all the gamma ray energies calculated from the electron energies were in agreement with the most accurate gamma-ray measurement within experimental error. This error is estimated to be less than or equal to the difference in K electron binding energies of neighbouring elements in most cases. The good agreement of the charge assignments with ^{252}Cf [sf] four parameter experiments in which X-ray selection was used for charge assignment [1,2,3] gives confidence in the above procedure, which is based on self consistency in the results of three and two parameter gamma-ray and X-ray experiments and the electron measurements. The method used is particularly useful for cases where the isotopic or X-ray yields are low or background problems severe.

The results of the analysis of the data are tabulated in table 2. Columns 1 and 2 give the mass and charge assignment for each electron line, or the most probable charge if no corresponding gamma ray line has been observed previously. Column 3 gives the energy of the electron line. Column 4 gives the best value of the corresponding gamma ray energy and refers to other observations of the gamma ray. Column 5 gives the calculated K line energies using the gamma ray energies of column 4 and the charge assignments of column 2.

The electron line assignments are graded in four categories in column 6. Explanatory information pertaining to the various categories is as follows:

Category A : In this category are those transitions whose mass and charge assignments appear to be established. The mass assignments in this category are based on two criteria. First, that the lines were well resolved and their masses could be well determined in the present experiment. A second restriction was that the masses so determined were either in good agreement with the mass assigned to the corresponding gamma ray in the present or a previous work, or that the neighbouring masses could be excluded on physical grounds. For example certain assignments could be ruled out on yield considerations. In other cases the fact that a relatively intense electron line clearly did not fit into the ground state rotational bands of adjacent even nuclei provided additional support for its assignment to a odd mass nucleus in between. The charge assignments are based on the comparison of the calculated and experimental values of the gamma-ray energies and good agreement with an X-ray selection experiment[11,12,1,2] as outlined above.

Category B: In this category the charge assignments are expected to be correct and are based on the same restrictions as for category A. The mass assignments have an error of $\pm$ 1 a.m.u. or as specified in column 1. The mass assignments are based only on the mass determination of the present work.

Category C: In this category the mass assignments are expected to have an error of $\pm$ 1 a.m.u. or as specified. The atomic numbers have been assigned based on gamma ray measurements but may be uncertain by $\pm$ 1 units of charge or as specified, due to mixing with another line or other ambiguities.

Category D: In this category are those transitions for which no corresponding gamma ray lines could be found. The mass assignments for these lines are expected to have an error of $\pm$ 1 a.m.u. or as specified and the atomic number values are those for the most probable charge[8] starting from the original, non-integral mass values derived.

The observations in column 7 include interpretations of certain lines, any mass or charge assignments proposed previously which differ from the present assignments, and other information of interest.

4. Discussion of Results

4.1 GENERAL FEATURES

As a result of these measurements a large number of transitions has been observed in both the lower and upper energy regions. While the gamma ray measurements revealed transitions predominantly in the 150 to 800 keV range of gamma-ray energies, the electron measurements were particularly selective of low energy transitions with electron energies from 30 to 300 keV. In fig. 7 the energies of the gamma ray transitions are averaged over certain mass regions and plotted as a function of mass. The gross energy tendency is consistent with what one would expect if the observed de-excitations of the primary fragments involved predominantly collective transitions. On physical grounds, it seems likely that the majority of the lines observed in the present measurements are linked with cascades from levels near the ground state since a necessary condition for the existence of high intensity transitions is that there be a high probability of populating the same levels each time a particular fission product is formed. Such conditions are unlikely to exist at high excitation energies.

The proposed interpretations of table 1 show that the more intense gamma-ray lines belong to transitions in the ground state bands of the even nuclei. In the electron measurements the situation is slightly different since the observed transition are selective of low energies. In regions away from nuclear deformation the

level spacing near the ground state in the even nuclei is not low enough to give rise to highly converted transitions. For this reason a large number of the observed transitions, particularly away from the regions of deformation, arise from the odd or odd-mass nuclei. However, near regions of nuclear deformation, where the level spacing in the ground state bands of the even nuclei is low enough, the corresponding lines stand out clearly in the electron spectra.

A further observation with regard to fig. 7 is that if the average energy of gamma rays may be regarded as an indication of nuclear stiffness over the averaged mass regions, then certain regions of hard nuclei e.g. around masses 88 to 90 and masses 130 - 132 and of soft nuclei e.g. near mass 100 and beyond mass 142, are clearly apparent. Very similiar features may be seen in fig. 8 which shows the relative yield of electrons per fragment. The curve was obtained by summing the events in each mass sorted electron spectrum over energy and dividing by the respective mass yields as obtained from the two parameter experiment described in subsect. 2.2. The error bars indicate the statistical errors in the yield curve. The gross features of the yield as a function of mass may be understood in terms of the nuclear deformations beyond mass 144, of the postulated[17] deformations of neutron rich nuclei near mass 107, and the closed shell properties of nuclei near mass 132. In the regions of deformation, with low level spacing in the ground state rotational band one would expect low energy transitions which are highly converted and therefore high electron yields, as seen in the yield curve. The reverse would apply in the closed shell regions. Moreover, there appears to be evidence of softness to deformation also around mass 100, in agreement with the low average gamma-ray energies observed in this mass region. This is of particular interest in view of the calculations of Arseniev et. al.[18] which predict deformation in this region.

4.2. TRANSITIONS IN THE EVEN NUCLEI

A general feature of both the electron and gamma ray spectra was the existence of certain very prominent lines which were often an order of magnitude stronger than the neighbouring lines. In most cases they could be assigned to the ground state

bands of even nuclei. Many of these transitions have also been observed in the ^{252}Cf [sf] experiments[1,2,3]. Apart from the indications from their mass and charge assignments, there are several other features which confirm their assignment to the ground state bands of the even nuclei. Thus for example, the relative intensities of those transitions which were assigned as $2^+ \rightarrow 0^+$, after they had been corrected for internal conversion, were found to be proportional to the independent yields of the isotopes to which the transitions were assigned. This is to be expected since it is known that the de-excitation in doubly even fragments, starting from high angular momentum, is channeled through the $2^+ \rightarrow 0^+$ transitions and therefore the intensity of these transitions should be similiar to the isotopic yields of the fragments concerned. Recently an analysis has been performed based on the statistical nature of the de-excitation of the fission fragments and the removal of their primary spin by Wilhelmy et. al.[19] which confirms that 95 to 98 per cent of the isotopic yield will be represented as $2^+ \rightarrow 0^+$ ground state band transitions. Confirmation for the assignments of a number of the transitions was also provided by the K/L ratios observed, which were consistent with E2 transitions. Table 3 lists the electron and gamma-ray lines assigned to the ground state bands of the doubly even isotopes. The measured K/L ratios and relative intensities of the gamma-ray lines are also given in the table. The "predicted intensities" given in column 5 are the calculated independent yields[8] corrected for converted transitions[20]. The units are arbitrary since it is the relative variation of the experimental and predicted intensities which is of interest. The discrepancy between the experimental and predicted intensities for ^{134}Te [$2^+ \rightarrow 0^+$] transitions is due to the fact that an appreciable feeding of the 1278 keV level proceeds via a 162 nsec isomeric state[9].

Many of the transitions listed in table 3 have been observed previously in the ^{252}Cf [sf] experiments of Cheifetz et. al.[1,2]. The present ^{235}U [n,f] measurements support their proposed assignments in all cases and the observed K/L ratios provide additional confirmation.

4.3 SPECIAL FEATURES

An interesting aspect of the present results is their relation to the deformed regions in the light and heavy fragment groups. Of particular interest is the region of transition from undeformed to deformed nuclei. The transition from spherical to deformed behaviour is characterised by a rapid drop in the energy of the first 2^+ level and an increase in the E_{4+}/E_{2+} energy ratio. As this ratio approaches 3.33, the value for a rigid rotator, the energy of the first 2^+ state changes less and less from isotope to isotope. Although it is not possible to determine the existence of static deformations from observed energy levels alone, studies of such systematics are good indicators of nuclear softness.

The first 2^+ levels for the nuclei in the region of postulated deformations in the light fragments are shown in fig. 9, which is based on present results and previous determinations[21]. Also plotted are the values of $[E_{2+}]_{critical}$ $[= 13\,\hbar^2/\mathcal{J}_{rigid}]$ for each mass value for purposes of comparison. This quantity is proposed as an approximate criterion of deformation by Alder et.al.[22]. According to this criterion nuclei having $E_{2+} > [E_{2+}]_{crit.}$ are to be assumed as spherical and those with $E_2 < [E_{2+}]_{crit.}$ as deformed.

If strong changes in the energy of the first 2^+ levels may be regarded as indicative of transitions from the vibrational to rotational modes and of a strong change in nuclear softness, then it appears that this transition occurs between neutron numbers 58 to 60 for the light fragments. This conclusion is also supported by the $[E_{2+}]_{crit.}$ criterion. Furthermore, although the transition in nuclear behaviour is analogous to that observed in the heavy fragment region[2] between neutron numbers 88 and 90, in the light fragments it is far more drastic. The most striking case is that of the zirconium isotopes [Z = 40] first observed by Cheifetz et.al.[1]. The energy of the first 2^+ level changes from 1223 keV for ^{98}Zr to 213 keV for ^{100}Zr. In the neighbouring Mo [Z = 42] and Sr [Z = 38] isotopes the changes in the first 2^+ level energies between N = 58 and 60 are much less abrupt and in Ru [Z = 44] the transition to rotational behaviour is relatively smooth and gradual. Sheline et.al.[23] have recently suggested that the drastic changes in nuclear characteristics in the Zr and Mo isotopes may be due to a highly deformed secondary minimum [associated with the deformed shell structure at Z = 40]

which moves down in energy with increasing N and becomes the ground state minimum at N = 60. Present results suggest that the behaviour of the Sr isotopes in the transition region may be similiarly interpreted. The theoretical calculations[23] however, have so far been unsuccessful in producing a second minimum for nuclei in the vicinity of $^{100}_{40}Zr$.

Two transitions of particular interest are the $2^+ \rightarrow 0^+$ transitions in ^{96}Sr and ^{98}Sr. The two isotopes, have a very low yield in ^{252}Cf [sf], however, in ^{235}U [n,f] they are produced in more significant quantities. The transitions are of importance for several reasons. The change from ^{96}Sr to ^{98}Sr is across the transition region [N = 58 to 60] and it is interesting to see how the first 2^+ levels of these isotopes fit into the systematics of fig. 9. Moreover the nuclei lie at the boundary of the deformed region and help to map the borderlines of the regions of deformation. Lastly, the calculations of Arseniev et.al.[18] predict that the strongest deformations should be in the heavier isotopes of strontium [98 - 102] and it is of interest to compare the results with their predictions.

In the present electron data, three different lines have been assigned to mass 98 ± 1 a.m.u., their electron energies being 157, 177 and 184 keV. The fact that corresponding lines have not been observed in ^{252}Cf [sf] experiments suggests that they originate from Sr rather from Y or Zr which have a higher yield for ^{252}Cf [sf]. The best candidate for the assignment as the $2^+ \rightarrow 0^+$ line in ^{98}Sr out of these appears to be the 177 keV electron line. This is so because a corresponding gamma ray line at 193 keV and mass 98 ± 1 has also been observed in the gamma ray experiment of the present work, whose energy is in agreement with the assignment of the electron line to Sr [see table 2]. Moreover, the relative intensity of the corresponding gamma ray is compatible with its being the $2^+ \rightarrow 0^+$ line in ^{98}Sr as may be seen in table 3.

In accordance with current theory it would be preferable to characterize a nucleus on the basis of the VMI[24] model but for this a knowledge of at least two experimentally determined parameters [e.g. E_{2^+} and E_{4^+}] is necessary. In the case of ^{98}Sr the only information available at present is the energy of the first 2^+

level in the ground state band, if the assignment proposed for the 193 keV gamma-ray is valid. Nevertheless, considerable understanding of the behaviour of a nucleus may be obtained by means of a number of indicators based on the energy of the first 2^+ level. It is therefore of interest to compare such indicators for neighbouring transition nuclei [i.e. nuclei with N = 60] in the light fragment group. One such indicator of deformation is the parameter $\chi (= [79.51/E_{2^+}] \times [158/A]^{5/3})$ which gives an approximate mass independent comparison of the energies of the first 2^+ states using the deformed nucleus ^{158}Gd as a comparison. Another useful comparison might be to obtain a relative value of the deformation [ß'] for the neighbouring transition nuclei ^{98}Sr, ^{100}Zr, ^{102}Mo, ^{104}Ru, using the centrifugal stretching model of Diamond et.al.[25] in which the moment of intertia $\mathcal{I}$ is assumed to be equal to $3 B ß^2$. A final indicator might be the energy difference between E_{2^+} and $[E_{2^+}]_{crit.}$ mentioned above. The values of these indicators for the four transition nuclei as well as ^{158}Gd are given in table 4. The ß' values were arrived at by calculating the moment of inertia $\mathcal{I}$ for each nucleus from the E_{2^+} value and then obtaining the value of ß' from the curve of $\mathcal{I}/[2/5\ AMR_o^2]$ versus ß of Diamond et.al. Also given in table 4 are theoretical values of the deformation parameter ß from the calculations of Arseniev et.al.[18], whose reported ε_o deformation has been converted to ß by the relation $ß \approx \varepsilon_o / 0.95$. The negative sign in the theoretical values implies oblate deformations. The last column of table 4 shows the experimental values of ß as derived from the B [E2] data for those nuclei whose B [E2] values are available.[1]

An examination of table 4 shows that the values of the deformation indicators for the nuclei in the postulated region of deformation in the light fragments are quite comparable with the values for ^{158}Gd which is known to be a good example of a deformed nucleus in the rare earth region. Furthermore, all three indicators suggest that of the four transition nuclei [N = 60] ^{98}Sr has the strongest tendency towards deformation, the tendency decreasing monotonically in the N = 60 nuclei as one moves towards ^{104}Ru. This is in good agreement with the theoretical predictions of Arseniev et.al. Moreover the ß' values derived in accordance with the procedure

outlined above are very similiar in magnitude and, more important, in variation to the calculated values for ß of Arseniev et.al.. However, the actual values of ß as obtained from the B[E2] values are somewhat higher in magnitude.

A final point of interest is the lack of transitions from the isotopes of technecium in the present work in comparison with the ^{252}Cf [sf] data. This is particularly significant in the electron data which cover the low energy transitions. The lack of transitions from Tc isotopes may be connected with nuclear shell effects in fission. Thus, if there is a tendency to converse 50 protons in the heavy fragments, then the primary yields of indium isotopes [Z = 49] and of their complementary fragments should be low. In ^{235}U [n,f] these complementary fragments consist of the technecium isotopes [Z = 43].

5. Conclusion

The experiments described have demonstrated that despite additional experimental difficulties the multiparameter measurements of the prompt radiations from primary fragments can be successfully extended to neutron induced fission. This makes it possible to investigate the mass region where the yield in spontaneous fission is low. It appears especially promising to use ^{233}U in such investigations since the mass regions covered in ^{233}U [n,f] partly overlap those reached in [t,p] reactions. Thus a large and continuous region of neutron rich nuclei in the nuclide chart is accessible for investigations.

Moreover, as a results of the present work and previous investigations it is now possible to assign a number of transitions to specific isotopes although in other cases some ambiquities in mass or charge assignments remain. The ground state bands of many of the doubly even fragments have been constructed[1,2]. The more complex but important decay schemes of the odd and odd-mass nuclei remain to be tackled. This is a difficult task since the structure is complicated and the number of nuclei is large. However, a start has been made by the assignment of a large number of lines and it remains to perform [γ-γ], [γ- e] and other coincidence studies in depth.

Acknowledgements

The authors would like to express their appreciation to Dr. John Wood, Dr. F. Dickmann and several colleagues from the Institut für Angewandte Kernphysik for stimulating discussions. We are also thankful to Miss I. Piper for experimental assistance. One of the authors [T.A.K.] wishes to express his thanks to the Gesellschaft für Kernforschung mbH, Karlsruhe and the Pakistan Atomic Energy Commission through whose collaboration his contribution to this work was made possible.

Appendix

METHOD OF CALCULATION OF THE FISSION FRAGMENT MASSES

It seems worthwhile to outline briefly the mass assignment procedure used here which is based upon some simplifications applied to the usual method. The simplified procedure saves computer time and the excellent agreement of the results with those from ^{252}Cf [ref. [1,2]], where no simplifications were applied, has proved its feasibility.

The energies of the fission fragments in detector 1 and 2 were calculated from the channel numbers x_i, using the equations for the mass dependent pulse-height calibration:

$$E_i = [a_i + a'_i \, m_i] x_i + b_i + b'_i \, m_i \qquad i = 1,2 \qquad [1]$$

m_i is the post-neutron emission mass. The calibration constants a_i, a'_i, b_i, b'_i, were deduced from the fragment energy single spectra in the well known manner[26]. According to ref.[26] provisional masses μ_i were defined on the basis of the following relationsships

$$\mu_1 E_1 = \mu_2 E_2 \qquad [2]$$

$$\mu_1 + \mu_2 = A_F \qquad [3]$$

where A_F is the mass of the fissioning nucleus. In the event by event calculation random numbers between -0.5 and +0.5 were added to each pulse height x_i in order to smoothen the pattern of the ADC channels. In addition in equation [1] m_i was replaced by μ_i. This introduces only a small error of about 0.2 MeV due to the small coefficients of the mass dependent terms. Using equations [1], [2] and [3] the provisional mass μ_1 and μ_2 were calculated from the relations

$$\mu_1 = A_F \cdot E_2/[E_1 + E_2] \text{ and}$$
$$\mu_2 = A_F - \mu_1 \qquad [4]$$

Instead of applying the neutron correction to each single event, the data were sorted according to the provisional mass μ yielding 48 gamma-ray spectra. The correlation between the provisional masses and the final masses m_1 and m_2 was then calculated using the equations[27]

$$\mu_1 \approx m_1^* \left[1 + \xi_1 \frac{m_2^*}{A_F}\right] \qquad [5]$$

$$m_1 = m_1^* - \nu_1 \qquad [6]$$

$$\xi_1 = \frac{\nu_1}{m_1} - \frac{\nu_2}{m_2} \qquad [7]$$

$$m_1^* + m_2^* = A_F \qquad [8]$$

m_1^* and m_2^* are the pre-neutron emission masses and ν_1 and ν_2 the mean number of prompt neutrons from fragments 1 and 2 respectively. These were taken from ref.[28] for the gamma-ray work and from ref.[29] for the later electron work. In this procedure the variation of ν with the kinetic energy of the fragments was neglected. This seemed to be justified by the observation that in $^{235}U[n,f]$ the mean number of prompt neutrons varies less than $\pm$ 0.5 mass units for total kinetic energies within the double variance around the average total kinetic energy[26,28]. This deviation is small compared to the typical mass resolution in this experiment of about 5 atomic mass units FWHM.

References

1] E. Cheifetz, R.C. Jared, S.G. Thompson and J.B. Wilhelmy, Phys. Rev. Letters 25, [1970], 38

2] J.B. Wilhelmy, S.G. Thompson, R.C. Jared and E. Cheifetz, Phys. Rev. Letters 25, [1970], 1122

3] R.L. Watson, J.B. Wilhelmy, R.C. Jared, C. Rugge, H.R. Bowman, S.G. Thompson and J.O. Rasmussen, Nucl. Phys. A 141, [1970], 449

4] F. Horsch and W. Michaelis, in Proceedings of the Second Symposium on the Physics and Chemistry of Fission, [IAEA, Vienna/Austria, 1969] p. 527

5] F. Horsch, in Proceedings of the Conference on the Properties of Nuclei far from the region of Beta stability, [CERN, Leysin , Switzerland, 1970] Vol.2, p.917

6] T.A. Khan, D. Hofmann and F. Horsch in Proceedings of the European Conference on Nuclear Physics [Aix-en-Provence, France, 1972] Jour. de Phys., Paris, Vol. 2, p. 30

7] F. Horsch and I. Piper, Kernforschungszentrum Karlsruhe report KFK 1003 [1969]

8] A.C. Wahl, A.E. Norris, R.A. Rouse and J.C. Williams, in Proceedings of the Second Symposium on the Physics and Chemistry of Fission, [IAEA, Vienna, Austria, 1969] p. 813 and Private Communication

9] W. John, F.W. Guy and J.J. Wesolowski, Phys.Rev. C 2, [1970], 1451

10] A.G. Blair, J.G. Beery, E.R. Flynn, Phys.Rev.Letter 22, [1969], 470

11] F.F. Hopkins, G.W. Phillips, J.R. White, C.Fred Moore and P. Richard, Phys. Rev. C 4, [1971], 1927

12] F.F. Hopkins, J.R. White, G.W. Phillips, C.Fred Moore and P. Richard, Phys. Rev. C 5, [1972], 1015

13] T. Alvager, R.A. Naumann, R.F. Petry, G. Sidenius and T.D. Thomas, Phys. Rev. 167, [1968], 1105

14] J.B . Wilhelmy, University of California Lawrence Radiation Laboratory report UCRL-18978 [1969]

15] N. Trautmann, N. Kaffrell, H.W. Behlich, H. Folger, G. Herrmann and D. Hübscher, Radiochimica Acta, to be published

16] J.T. Larsen, W.L. Talbert and J.R. Mc Connell, Phys. Rev. C 3, [1971], 1372

17] S.A.E. Johansson, Arkiv för Fysik 36, Nr. 67 [1966], 599

18] D.A. Arseniev, A. Sobiczewski und V.G. Soloviev, Nucl. Phys. A 139, [1969], 269

19] J.B. Wilhelmy, E. Cheifetz, R.C. Jared, S.G. Thompson, H.R. Bowman and J.O. Rasmussen, to be published

20] L.A. Sliv and I.M. Band, in Alpha, Beta and Gamma-Ray Spectroscopy, edited by K. Siegbahn [North Holland Publishing Co., Amsterdam 1965], p. 1639

21] J.L. Wood, A Compilation and Survey of Data on Levels of Even-Even Nuclei Kernforschungszentrum Karlsruhe report KFK 1/71-1

22] K. Alder, A. Bohr, T. Huus, B. Mottelson and A. Winther, Rev. Mod. Phys. 28, [1956], 432

23] R.K. Sheline, I. Ragnarsson and S.G. Nilsson, Physics Lett. 41B, [1972], 115

24] M.A.J. Mariscotti, G.Scharff-Goldhaber and B.Buck, Phys. Rev. 178, [1969], 1864

25] R.M. Diamond, F.S. Stephens and W.J. Swiatecki, Phys. Lett. 11, [1964], 315

26] H.W. Schmitt, W.M. Gibson, J.H. Neiler, F.J. Walter and T.D. Thomas in Proceedings of the Symposium on the Physics and Chemistry of Fission [IAEA, Salzburg, Austria, 1965], Vol. 1, p. 531

27] H.W. Schmitt, J.H. Neiler, F.J. Walter, Phys. Rev. 141, [1966], 1146

28] V.F. Apalin, Yu. N. Gritsyuk, J.E. Kutinov, V.J. Lebedev, L.A.Mikaelian Nucl. Phys. 71, [1965], 553

29] E.E. Maslin, A.L. Rodgers, W.G.F. Core, Phys. Rev. 164, [1967], 1520

FIGURE CAPTIONS

Fig. 1 Schematic diagram of the arrangement for the gamma-ray experiment.

Fig. 2 Prompt gamma-ray spectra for the fragment mass ranges A_L = 88 - 90 and A_H = 143 - 145 [upper figure], and A_L = 102 - 104 and A_H = 130 -132 [lower figure]. The spectra demonstrate the dependence of the gamma-ray energy on the velocity and direction of the fragment motion. Each figure represents two cases:

a] Light fragments moving towards the gamma-ray detector, and

b] Heavy fragments moving towards the gamma-ray detector.

The letters L and H indicate some assignments to the light and heavy fragments respectively.

Fig. 3 Schematic diagram of the arrangement for the electron experiment.

Fig. 4 Block diagram of the electronics for the electron experiment.

Fig. 5 A mass sorted energy spectrum of internal conversion electrons from a mass interval in the light fragment group.

Fig. 6 A mass sorted energy spectrum of internal conversion electrons from a mass interval in the heavy fragment group.

Fig. 7 Averaged energies of the observed gamma-ray transitions as a function of mass A. The length of the horizontal bars gives the magnitude of the averaging interval.

Fig. 8 The relative yield of internal conversion electrons as a function of fission fragment mass.

Fig. 9 The systematic variation of the first 2^+ excited states in the doubly even isotopes of Kr, Sr, Zr, Mo, Ru. The unbroken line is a plot of $[\ E_{2+}\ ]_{critical}$ in this region [see text].

TABLE 1. ASSIGNMENT OF PROMPT GAMMA RAYS TO INDIVIDUAL FRAGMENTS FROM NEUTRON-INDUCED FISSION OF ^{235}U.

Fragment Mass A	Most Probable Charge Zp	Gamma-Ray Energy[a] E_γ[keV]	Relative Intensity experimental per fission and ~16mm flight path	Interpretation based upon systematics of $2^+ \rightarrow 0^+$ transitions in neighbouring even-even nuclei	Interpretation based upon close agreement of energy and mass assignment with ^{252}Cf data	Interpretation based upon close agreement of energy and mass assignment with [t,p] and beta-decay data
88 ± 1	35	869 ± 5	< 25			
91 ± 1	36	706 ± 4	70 ± 23	[$^{90}Kr/2^+ \rightarrow 0^+$/]		
		956 ± 5	32 ± 11	[$^{92}Kr/2^+ \rightarrow 0^+$/]		
93 ± 1	38	144 ± 2	14.5 ± 7.5			
95 ± 1	38	249 ± 2	6.9 ± 3.5			
		834 ± 4	61 ± 20	[$^{94}Sr/2^+ \rightarrow 0^+$/]		
96 ± 1	38/39	813 ± 4	80 ± 27	[$^{96}Sr/2^+ \rightarrow 0^+$/]		
96 ± 1	39	376 ± 3	25.5 ± 12.5			
96 ± 1	39	[427 ± 4][b]	[> 32]			
98 ± 1	40	* 193 ± 2	13.0 ± 4.5			
99 ± 1	40	* 123 ± 2	38 ± 19			
		* 157 ± 2	21 ± 7			
100 ± 1	40	* 98 ± 2	> 18		^{101}Zr	
		* 212 ± 2	37 ± 13		$^{100}Zr/2^+ \rightarrow 0^+$/	
		* 351 ± 3	56 ± 28		$^{100}Zr/4^+ \rightarrow 2^+$/	
		495 ± 3	55 ± 18		$^{100}Zr/6^+ \rightarrow 4^+$/	
		622 ± 5	50 ± 25		[$^{100}Zr/8^+ \rightarrow 6^+$/]	

Fragment Mass A	Most Probable Charge[a] Zp	Gamma-Ray Energy E_γ[keV]	Relative Intensity experimental per fission and ~16mm flight path	Interpretation based upon systematics of $2^+ \rightarrow 0^+$ transitions in neighbouring even-even nuclei	Interpretation based upon close agreement of energy and mass assignment with ^{252}Cf data	Interpretation based upon close agreement of energy and mass assignment with [t,p] and beta-decay data
$100 \pm \frac{1}{2}$	40	1224 ± 5	29 ± 15			$^{98}Zr/2^+ \rightarrow 0^+/$
101 ± 1	40/41	* 325 ± 3	16 ± 8		$^{102}Zr/4^+ \rightarrow 2^+/$	
102 ± 1	41	174 ± 2	7.7 ± 2.6			
		* 275 ± 2	7.6 ± 2.6			
103 ± 1	41	136 ± 2	7.8 ± 2.7			
		* 296 ± 2	8.8 ± 2.9		$^{102}Mo/2^+ \rightarrow 0^+/$	
		518 ± 3	15 ± 7.5		$^{104}Mo/6^+ \rightarrow 4^+/$	
103 ± 2	41	581 ± 4	15 ± 7.5		$^{102}Zr/8^+ \rightarrow 6^+/$	
104 ± 2	41/42	* 157 ± 2	5.4 ± 1.8			
104 ± 1	41/42	* 191 ± 2	12 ± 4		$^{104}Mo/2^+ \rightarrow 0^+/$	
		[556 ± 3][c]	[12 ± 6]			
	42	366 ± 3	15.5 ± 7.5		$^{104}Mo/4^+ \rightarrow 2^+/$	
131 ± 1	51	1222 ± 5	12.3 ± 6	[$^{130}Sn/2^+ \rightarrow 0^+/$]		
132 ± 1	51	965 ± 5	19.5 ± 10	$^{132}Te/2^+ \rightarrow 0^+/$		
134 ± 1	52	1180 ± 5	21 ± 10			
		1278 ± 5	34 ± 17	$^{134}Te/2^+ \rightarrow 0^+/$	$^{134}Te/2^+ \rightarrow 0^+/$	
135 ± 1	52/53	425 ± 3	40 ± 13			
138 ± 1	53/54	585 ± 4	106 ± 60		$^{138}Xe/2^+ \rightarrow 0^+/$	
139 ± 1	54	* 373 ± 3	70 ± 35		$^{140}Xe/2^+ \rightarrow 0^+/$	
		482 ± 3	112 ± 37			

Table 1 [conintued]

Fragment Mass	Most Probable[a] Charge	Gamma-Ray Energy	Relative Intensity experimental per fission and ~16mm flight path	Interpretation based upon systematics of $2^+ \rightarrow 0^+$ transitions in neighbouring even-even nuclei	Interpretation based upon close agreement of energy and mass assignment with ^{252}Cf data	Interpretation based upon close agreement of energy and mass assignment with [t,p] and beta-decay data
A	Zp	E_γ[keV]				
		723 ± 4	47 ± 23			
140 ± 1	54/55	* 283 ± 2	16.5 ± 5.5			[^{140}Cs]
141 ± 1	55	303 ± 3	12 ± 6			
		* 357 ± 3	36.5 ± 12		$^{142}Ba/2^+ \rightarrow 0^+$/	
141 ± 2	55	475 ± 3	51 ± 17			
141 ± 1	55	629 ± 4	38 ± 19			[^{140}Cs]
142 ± 1	56	429 ± 3	55 ± 27			
143 ± 1	56	* 115 ± 2	> 18			
		* 198 ± 2	36 ± 12		$^{144}Ba/2^+ \rightarrow 0^+$/	
		* 330 ± 3	57 ± 19		$^{144}Ba/4^+ \rightarrow 2^+$/	
		343 ± 3	23.5 ± 8			
143 ± 2	56	492 ± 4	31 ± 15			
143 ± 1	56	507 ± 3	27 ± 9		$^{144}Ba/6^+ \rightarrow 4^+$/	
		820 ± 5	45 ± 22			
144 ± 2	56	* 183 ± 2	12 ± 4			
146 ± 2	57/58	502 ± 3	$17,5 \pm 6$			
147 ± 1	58	* 294 ± 2	14 ± 5		$^{148}Ce/4^+ \rightarrow 2^+$/	

[a] Derived from the tables given in Ref. [8]

[b] The high energy Doppler shifted member is partly screened by another line.

[c] The spectra permit the alternative interpretation: $A = 130 \pm 1$, $Zp = 50$, $E_\gamma = 585 \pm 4$ keV, Rel. Int. $= 13 \pm 7$.

Table 1 [continued]

TABLE 2. ASSIGNMENT OF PROMPT ELECTRONS TO INDIVIDUAL FRAGMENTS

Mass Number	Atomic Number	Electron Energy [keV]	γ - ray Energy [keV]	K-line Energy with assigned Z	Assignment Category	Observations
89	35/36	165			D	
91	36/37	182			D	
93	37/38	143			D	
94	38	68			D	
94	37/38	177			D	
94	37/38	264			D	
94	37/38	268			D	
94	37/38	312			D	
94	37/38	347			D	
95	38	48			D	
95	38	100			D	
95	38	110			D	
95	39 Y	113	$130 \cdot 2^{c}$	$113 \cdot 2$	B	
96	39 Y	42	$58 \cdot 2^{c}$	$41 \cdot 2$	B	
96	39	71	$87 \cdot 6^{c}$	$70 \cdot 6$	C	
96	38/39	92			D	
96	38/39	165			D	
96	38/39	210			D	

Mass Number	Atomic Number		Electron Energy [keV]	γ - ray Energy [keV]	K-line Energy with assigned Z	Assignment Category	Observations
97	39	Y	62	79 · 9[c]	62 · 8	C	
97	39		332			D	
98	39/40		131			D	
98	39/40		157			D	Probably from Sr since not seen in ^{252}Cf [s,f]
98	38	Sr	177	193[e]	176 · 9	B	Suggested assignment ^{98}Sr $2^+ \rightarrow 0^+$
98	39/40		184			D	Probably from Sr since not seen in ^{252}Cf [s,f]
98	39/40		338			D	
98	39		362			D	
99	40	Zr	38	55 · 0[c]	37 · 0	B	
99^{+0}_{-1}	40^{+1}_{-0}		46	64 · 3[c]	46 · 3	C	
99	41	Nb	55	73 · 8[c]	55 · 0	B	
99	41	Nb	78	97 · 0[c,i]	78 · 0	A	
99	39	Y	84	100 · 6[c]	83 · 6	B	
99	39/40		87			D	
99	39	Y	105	122 · 3[c,e,f]	105 · 2	A	
99	41	Nb	119	138[i]	119	A	
99	39/40		126			D	
99	40	Zr	147	165 · 3[d]	147 · 3	B	
99	39/40		170			D	
100	41	Nb	64	84 · 0[c]	65 · 0	B	

Table 2 [continued]

Mass Number	Atomic Number		Electron Energy [keV]	γ - ray Energy [keV]	K-line Energy with assigned Z	Assignment Category	Observations
100	41	Nb	100	119 · 1[c]	100 · 1	B	
100	41	Nb	108	126 · 4[c]	107 · 4	C	
100	40		135			D	
100	41	Nb	139	159 · 0[d,e,i]	140 · 0	A	d assigns to complimentary fragment [La]
100	41	Nb	153	172 · 0[d]	153 · 0	B	
100	41	Nb	192	212 · 0[d]	193 · 0	B	
100	40	Zr	195	212 · 7[b,c,d,e]	194 · 7	A	$^{100}Zr\ 2^+ \rightarrow 0^+$
100	40	Zr	334	352 · 1[b,e]	334 · 1	A	$^{100}Zr\ 4^+ \rightarrow 2^+$
101	40	Zr	36	53 · 4[c]	35 · 4	B	
101	39	Y	74	91 · 0[c,f]	74 · 0	A	
101	40	Zr	81	98 · 2[c,e,g]	81 · 2	A	
101	40		110			D	
101	41	Nb	257	276 · 0[e,i]	257 · 0	A	
101	40/41		264			D	
102	40	Zr	133	151 · 9[b]	133 · 9	A	$^{102}Zr\ 2^+ \rightarrow 0^+$
102	40	Zr	309	326 · 6[b,e]	308 · 6	A	$^{102}Zr\ 4^+ \rightarrow 2^+$
102	42	Mo	275	296 · 0[b,e]	276 · 0	A	$^{102}Mo\ 2^+ \rightarrow 0^+$
102	41	Nb	279	297[i]	278	A	
104	41	Nb	122	140 · 9[c,f]	121 · 9	A	
104	42	Mo	173	192 · 3[b,e]	172 · 3	A	$^{104}Mo\ 2^+ \rightarrow 0^+$

Table 2 [continued]

Mass Number	Atomic Number		Electron Energy [keV]	γ- ray Energy [keV]	K-line Energy with assigned Z	Assignment Category	Observations
105	43	Tc	116	138[i]	117	C	
105	43	Tc	138	159[e,i]	138	C	
106	42	Mo	152	171 · 7[b]	151 · 7	A	^{106}Mo $2^+ \rightarrow 0^+$
106	42		165			D	
108	44	Ru	220	242 · 3[b]	220 · 2	A	^{108}Ru $2^+ \rightarrow 0^+$
133	53	I	196	228 · 5[c,i]	195 · 3	B	i assigns to mass 132
134	53	I	84	116 · 8[c]	83 · 6	B	
136	53	I	55	87 · 4[c,g]	54 · 2	B	
136	53	I	123	155 · 1[c,f]	121 · 9	B	b assigns to mass 137^{+0}_{-}
136^{+0}_{-1}	53	I	226	261 · 0[c,f]	227 · 8	B	b assigns to mass 135^{+0}_{-1}
136	53	I	256	288 · 4[c,f]	255 · 2	B	b assigns to mass 136^{+0}_{-1}
137^{+2}_{-0}	54		71	108 · 6[c]	71 · 2	C	Mixes with ^{143}Cs line at 69 keV
137^{+2}_{-0}	54	Xe	100	138 · 3[c]	100 · 9	B	
137^{+2}_{-0}	54	Xe	135	172 · 0[c]	134 · 6	B	
137	54	Xe	275	314 · 1[d,f]	276 · 7	A	
137	54	Xe	361	400 · 0[d,f]	362 · 6	B	f assigns to mass 138^{+0}_{-1}
138	55	Cs	103	138 · 3[c,h]	102 · 3	A	
138	55	Cs	119	154 · 1[c,h,i]	118 · 1	A	
139	54	Xe	38	74 · 2[c]	36 · 8	B	
$139^{+}_{-}2$	54	Xe	105	143 · 0[c]	105 · 6	B	
140	55	Cs	42	78 · 6[c,g]	42 · 6	A	
140	55	Cs	44	80 · 0[c,h]	44 · 0	B	

Table 2 [continued]

Mass Number	Atomic Number		Electron Energy [keV]	γ- ray Energy [keV]	K-line Energy with assigned Z	Assignment Category	Observations
140	55	Cs	183	$219 \cdot 0^{c,f,i}$	$183 \cdot 0$	A	i assigns to mass 139,
140	55	Cs	251	$287 \cdot 4^{c,e}$	$251 \cdot 4$	B	
141	55	Cs	36	$71 \cdot 5^{c,h}$	$35 \cdot 5$	B	
141	55	Cs	46	$81 \cdot 7^{c,h}$	$45 \cdot 7$	A	
141^{+1}_{-0}	55	Cs	49	$84 \cdot 2^{c}$	$48 \cdot 2$	B	
141	55	Cs	53	$89 \cdot 0^{c,h}$	53	A	
141	56	Ba	65	$102 \cdot 5^{c,h}$	$65 \cdot 1$	B	
141	55	Cs	280	$315 \cdot 3^{c}$	$279 \cdot 3$	B	
141^{+0}_{-2}	54	Xe	340	$376 \cdot 8^{a,e}$	$339 \cdot 4$	B	Probably ^{140}Xe $2^{+} \rightarrow 0^{+}$ mixing with another line
142	55	Cs	55	$91 \cdot 4^{c,h}$	$55 \cdot 4$	A	
142	55	Cs	60	$96 \cdot 9^{c,f}$	$60 \cdot 9$	A	
142	55	Cs	156	$191 \cdot 8^{c,i,k}$	$155 \cdot 8$	A	
142	57	La	192	$231 \cdot 6^{d,i,k}$	$192 \cdot 7$	A	
142	54	Xe	300	$335 \cdot 8^{d,h}$	$298 \cdot 4$	B	
142	56	Ba	322	$359 \cdot 7^{a,d,e}$	$322 \cdot 0$	A	^{142}Ba $2^{+} \rightarrow 0^{+}$
143^{+0}_{-2}	55	Cs	69	$106 \cdot 0^{c,h}$	$70 \cdot 0$	B	mixing with ^{137}Xe line at 71 keV
143	56	Ba	75	$112 \cdot 4^{c,e,g,h}$	$75 \cdot 0$	B	g assigns to mass 144; h to mass 141
143	56	Ba	81	$117 \cdot 4^{c,f,h}$	$80 \cdot 0$	A	f assigns $144^{\pm}1$; h assigns to mass 142
143	56	Ba	101	$137 \cdot 9^{c,h}$	$100 \cdot 5$	B	h assigns to mass 141
143	56	Ba	175	$212 \cdot 4^{d}$	$174 \cdot 6$	B	

Table 2 [continued]

Mass Number	Atomic Number		Electron Energy [keV]	γ - ray Energy [keV]	K-line Energy with assigned Z	Assignment Category	Observations
144^{+2}_{-1}	57		40	77 · 6[c]	38 · 7	C	interference from ^{139}Xe line at 38 keV
144^{+2}_{-1}	57		45	84 · 0[c]	45 · 1	C	interference from ^{140}Cs line at 44 keV
144	56	Ba	162	199 · 4[a,d,e]	161 · 9	A	^{144}Ba $2^+ \rightarrow 0^+$
144	57		232	270 · 5[d]	231 · 6	C	interference from another line near mass 137
144	56	Ba	293	331 · 0[a,e]	293 · 6	A	^{144}Ba $4^+ \rightarrow 2^+$
144	57	La	349	388 · 5[d,i]	349 · 8	B	
144	58	Ce	357	397 · 5[a,d]	357 · 2	A	^{144}Ce $2^+ \rightarrow 0^+$
145	57	La	62	100 · 3[c,g]	61 · 4	A	
145	57	La	66	104 · 3[c,f]	65 · 4	B	
145^{+2}_{-0}	58	Ce	78	117 · 8[c]	77 · 4	B	
145	57	La	111	150 · 4[c]	111 · 5	B	
145	57	La	114	153 · 8[c]	115 · 1	B	
145	57	La	128	167 · 7[c,f]	128 · 8	B	
145^{+2}_{-0}	58		130	171 · 9[d]	131 · 6	C	
145^{+2}_{-0}	58		201	240 · 6[d]	200 · 2	C	
146	57	La	43	82 · 2[c,f]	43 · 3	A	
146	57	La	91	130 · 5[c,f,g]	91 · 7	A	
146	56	Ba	144	181 · 4[a,c,e,f,g]	144 · 0	A	^{146}Ba $2^+ \rightarrow 0^+$; g,e assign mass $144^{+}_{-}1$, f assigns $145^{+}_{-}1$
146	58	Ce	218	258 · 4[a,d]	218 · 2	A	^{146}Ce $2^+ \rightarrow 0^+$
146	56	Ba	296	333 · 0[a]	295 · 6	A	^{146}Ba $4^+ \rightarrow 2^+$

Table 2 [continued]

Mass Number	Atomic Number		Electron Energy [keV]	γ - ray Energy [keV]	K-line Energy with assigned Z	Assignment Category	Observations
147 ± 2	58		159	199 · 8[d]	159 · 4	C	
147	58	Ce	242	283 · 8[d,f]	243 · 4	A	
148	58	Ce	118	158 · 8[a,d,f]	118 · 4	A	^{148}Ce $2^+ \rightarrow 0^+$
148	58	Ce	255	295 · 6[a,d,e]	255 · 3	A	^{148}Ce $4^+ \rightarrow 2^+$
148	58	Ce	346	386 · 2[a]	345 · 8	B	^{148}Ce $6^+ \rightarrow 4^+$, weak line
149	58	Ce	94	134 · 0[c,f]	93 · 6	A	
149	58	Ce	102	142 · 7[c,f,g]	102 · 3	A	g assigns to ^{149}Pr
150	58	Ce	58	97 · 7[a,c]	57 · 3	A	^{150}Ce $2^+ \rightarrow 0^+$
150	58	Ce	170	209 · 0[a]	168 · 6	A	^{150}Ce $4^+ \rightarrow 2^+$
152	60	Nd	32	75 · 9[a]	32 · 3	A	^{152}Nd $2^+ \rightarrow 0^+$
152	60	Nd	121	164 · 7[a]	121 · 1	A	^{152}Nd $4^+ \rightarrow 2^+$

Table 2 [continued]

[a] See Ref. 2
[b] See Ref. 1
[c] See Ref. 11
[d] See Ref. 12
[e] See table 1
[f] See Ref. 9
[g] See Ref. 3
[h] See Ref. 13
[i] See Ref. 14
[i] See Ref. 15
[k] See Ref. 16

TABLE 3. GROUND STATE BAND TRANSITIONS IN THE DOUBLY EVEN FISSION PRODUCTS OF $^{235}U[n,f]$

Isotope	Interpretation	Gamma-Ray Energy keV	Relative Intensity		Experimental		K/L Ratio	
			Experimental per fission and ~16mm flight path	Predicted incl. correction for Int. Conversion	K-line Energy keV	L-line Energy keV		
^{90}Kr	$[2^+ \rightarrow 0^+]$	706 ± 4	70 ± 23	55				
^{92}Kr	$[2^+ \rightarrow 0^+]$	956 ± 5	32 ± 11	28				
^{94}Sr	$[2^+ \rightarrow 0^+]$	834 ± 4	61 ± 20	59				
^{96}Sr	$[2^+ \rightarrow 0^+]$	813 ± 4	80 ± 27	25				
^{98}Sr	$[2^+ \rightarrow 0^+]$	193 ± 2	13 ± 4.5	8	177	191	6	Suggest E2 transitions
^{98}Zr	$2^+ \rightarrow 0^+$	1224 ± 5	29 ± 15	45				
^{100}Zr	$2^+ \rightarrow 0^+$	212 ± 2	37 ± 13	52	195	210	7	Suggest E2 transitions
^{100}Zr	$4^+ \rightarrow 2^+$	351 ± 3			334			
^{102}Zr	$2^+ \rightarrow 0^+$				133	150	6	Suggest E2 transitions
^{102}Zr	$4^+ \rightarrow 2^+$	325 ± 3			309			
^{102}Mo	$2^+ \rightarrow 0^+$	296 ± 2	8.8 ± 2.9	12	275			
^{104}Mo	$2^+ \rightarrow 0^+$	191 ± 2	12 ± 4	12	173	188	5.6	Consistent with E2
^{104}Mo	$4^+ \rightarrow 2^+$	366 ± 3						
^{106}Mo	$2^+ \rightarrow 0^+$				152	170	5	Consistent with E2
^{130}Sn	$[2^+ \rightarrow 0^+]$	1222 ± 5	12.3 ± 6	16				
^{132}Te	$2^+ \rightarrow 0^+$	965 ± 5	19.5 ± 10	16				
^{134}Te	$2^+ \rightarrow 0^+$	1278 ± 5	34 ± 17	82				
^{138}Xe	$2^+ \rightarrow 0^+$	585 ± 4	106 ± 60	43				
^{140}Xe	$2^+ \rightarrow 0^+$	373 ± 3	70 ± 35	49	340			

Isotope	Interpretation	Gamma-Ray Energy keV	Relative Intensity Experimental per fission and ~16mm flight path	Relative Intensity Predicted incl. correction for Int. Conversion	Experimental K-line Energy keV	Experimental L-line Energy keV	K/L Ratio	
^{142}Ba	$2^+ \rightarrow 0^+$	357 ± 3	36.5 ± 12	43	322	356	5.2	Consistent with E2
^{144}Ba	$2^+ \rightarrow 0^+$	198 ± 2	36 ± 12	38	162	195	3.7	Consistent with E2
^{144}Ba	$4^+ \rightarrow 2^+$	330 ± 3			293			
^{146}Ba	$2^+ \rightarrow 0^+$	183 ± 2	12 ± 4	7	144	176	2.7	Consistent with E2
^{146}Ba	$4^+ \rightarrow 2^+$				296			
^{146}Ce	$2^+ \rightarrow 0^+$				218	252	4.0	Consistent with E2
^{148}Ce	$2^+ \rightarrow 0^+$				118	153	2.8	Consistent with E2
^{148}Ce	$4^+ \rightarrow 2^+$	294 ± 2			255	290		
^{150}Ce	$2^+ \rightarrow 0^+$				58	91	1.8	Consistent with E2
^{150}Ce	$4^+ \rightarrow 2^+$				170			

Table 3 [continued]

TABLE 4. DEFORMATION INDICATORS FOR THE TRANSITION NUCLEI IN THE LIGHT FRAGMENT GROUP.

NUCLEUS	NEUTRON NUMBER	E_{2+} keV	$[E_{2+}]_{crit}$ keV	$[E_{2+}]_{crit} - E_{2+}$	X	ß′	ß [Theoretical][b]	ß [Experimental][c]
^{98}Sr	60	193	422	229	0.92	0.30	- 0.31	
^{100}Zr	60	213	408	195	0.80	0.28	- 0.29	0.364
^{102}Mo	60	296	395	99	0.56	0.23	[- 0.28][d]	0.348
^{104}Ru	60	358[a]	383	25	0.45	0.21	[- 0.26][d]	
^{158}Gd		79.5[a]	192	112	1.0	0.24		0.24

[a]See ref. 21 [b]See ref. 18 [c]See ref. 1 [d]deduced from fig. 4 of ref. 18

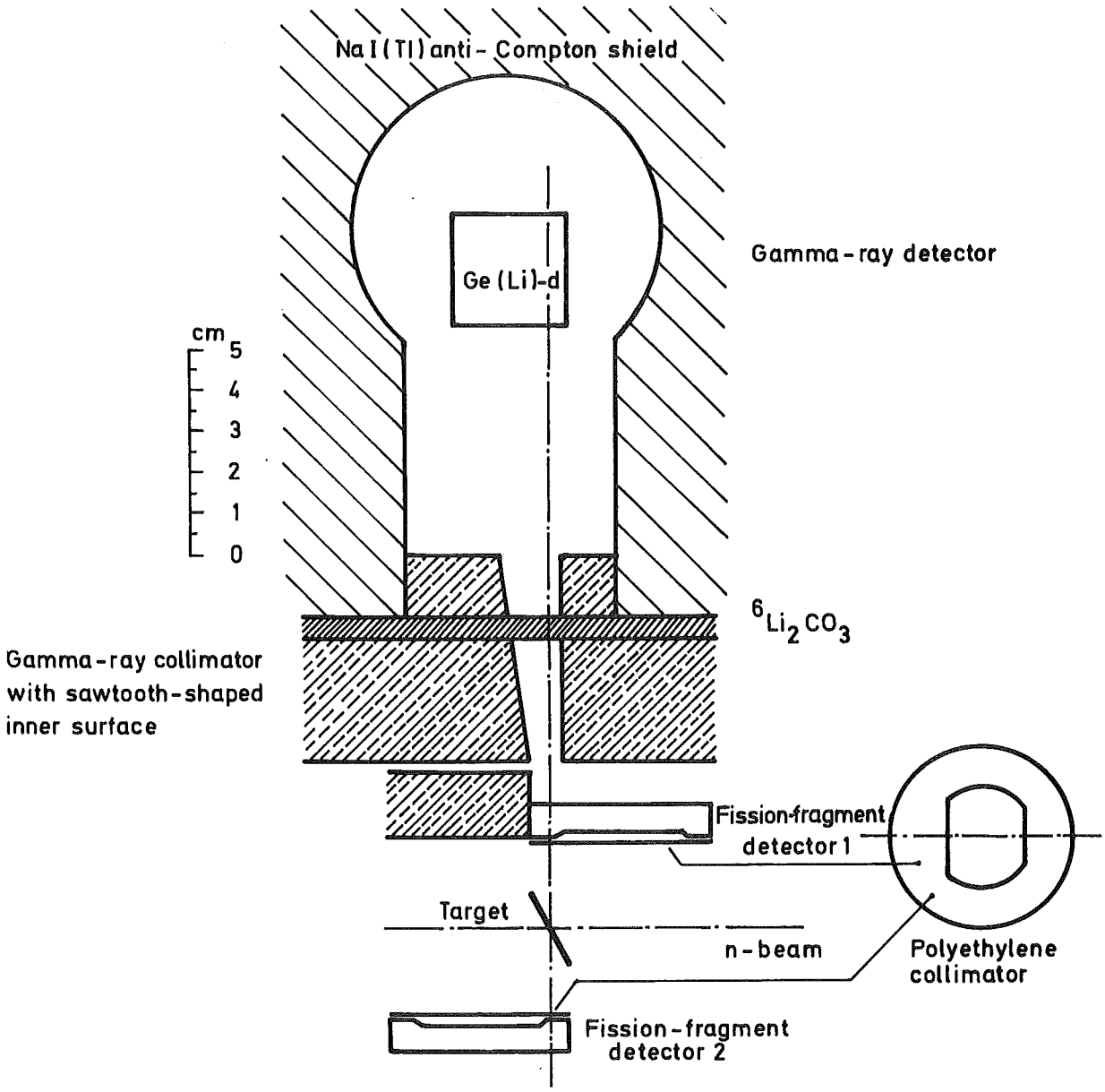
NaI(Tl) anti-Compton shield
Ge(Li)-d
Gamma-ray detector
cm
5
4
3
2
1
0
$^6Li_2CO_3$
Gamma-ray collimator
with sawtooth-shaped
inner surface
Fission-fragment
detector 1
Target
n-beam
Polyethylene
collimator
Fission-fragment
detector 2

Fig. 1

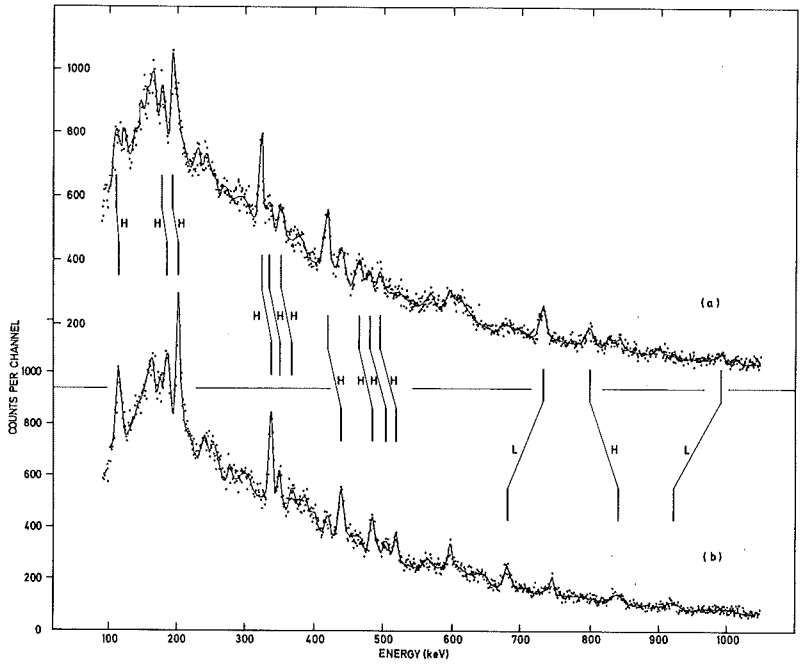
COUNTS PER CHANNEL
ENERGY (keV)
(a)
(b)
H
L

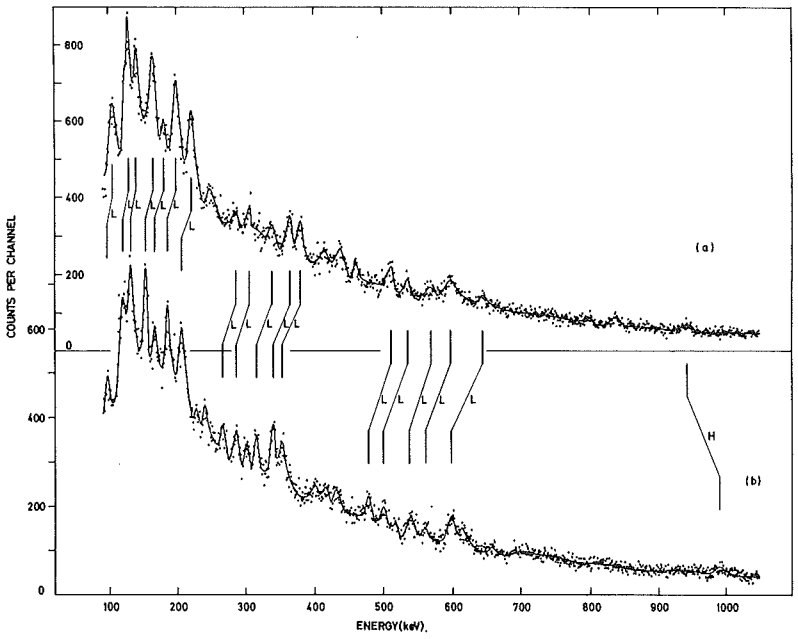
COUNTS PER CHANNEL
ENERGY(keV)
(a)
(b)
L
H

Fig. 2

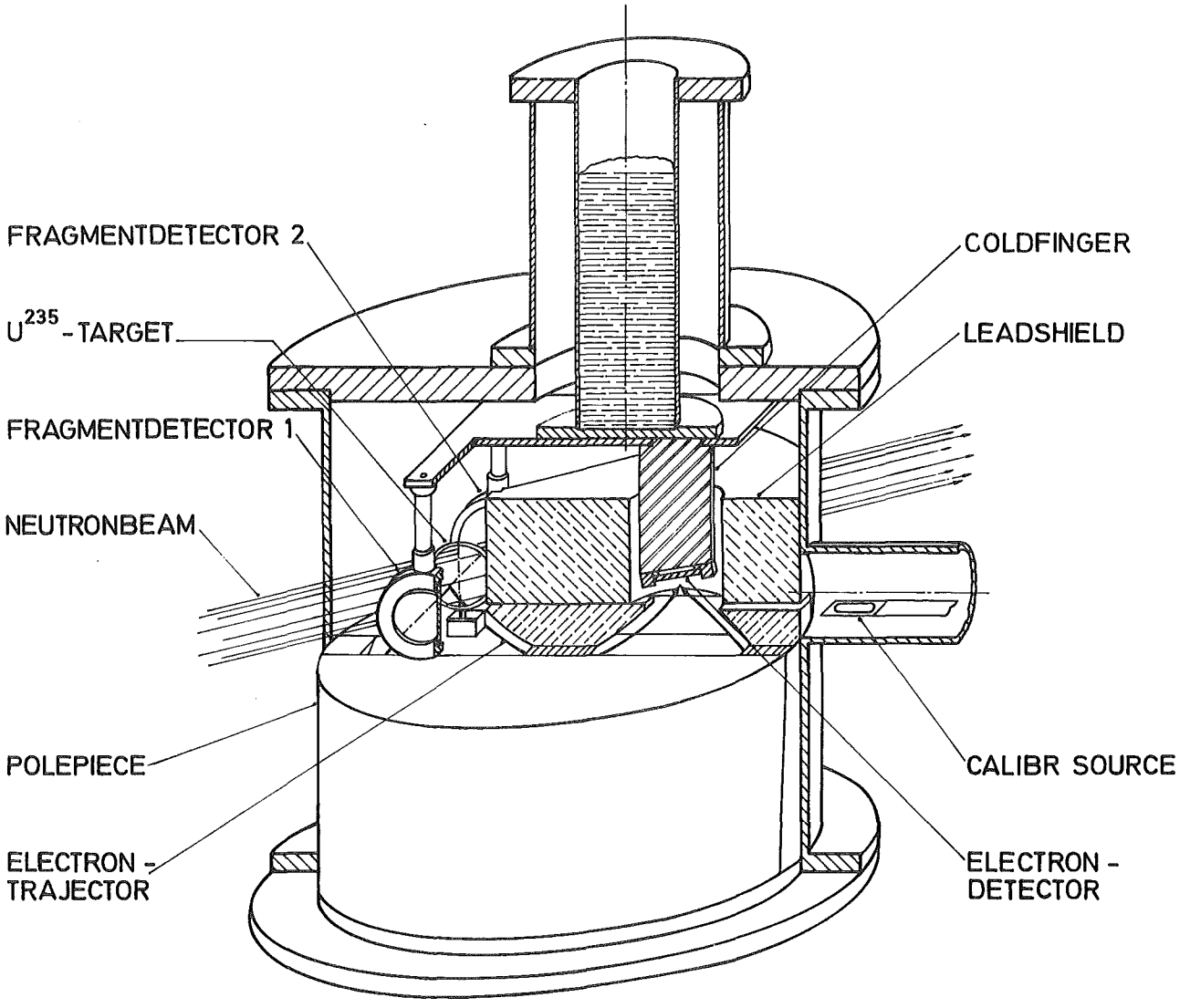
FRAGMENTDETECTOR 2
U^{235}-TARGET
FRAGMENTDETECTOR 1
NEUTRONBEAM
POLEPIECE
ELECTRON - TRAJECTOR
COLDFINGER
LEADSHIELD
CALIBR SOURCE
ELECTRON - DETECTOR

Fig. 3

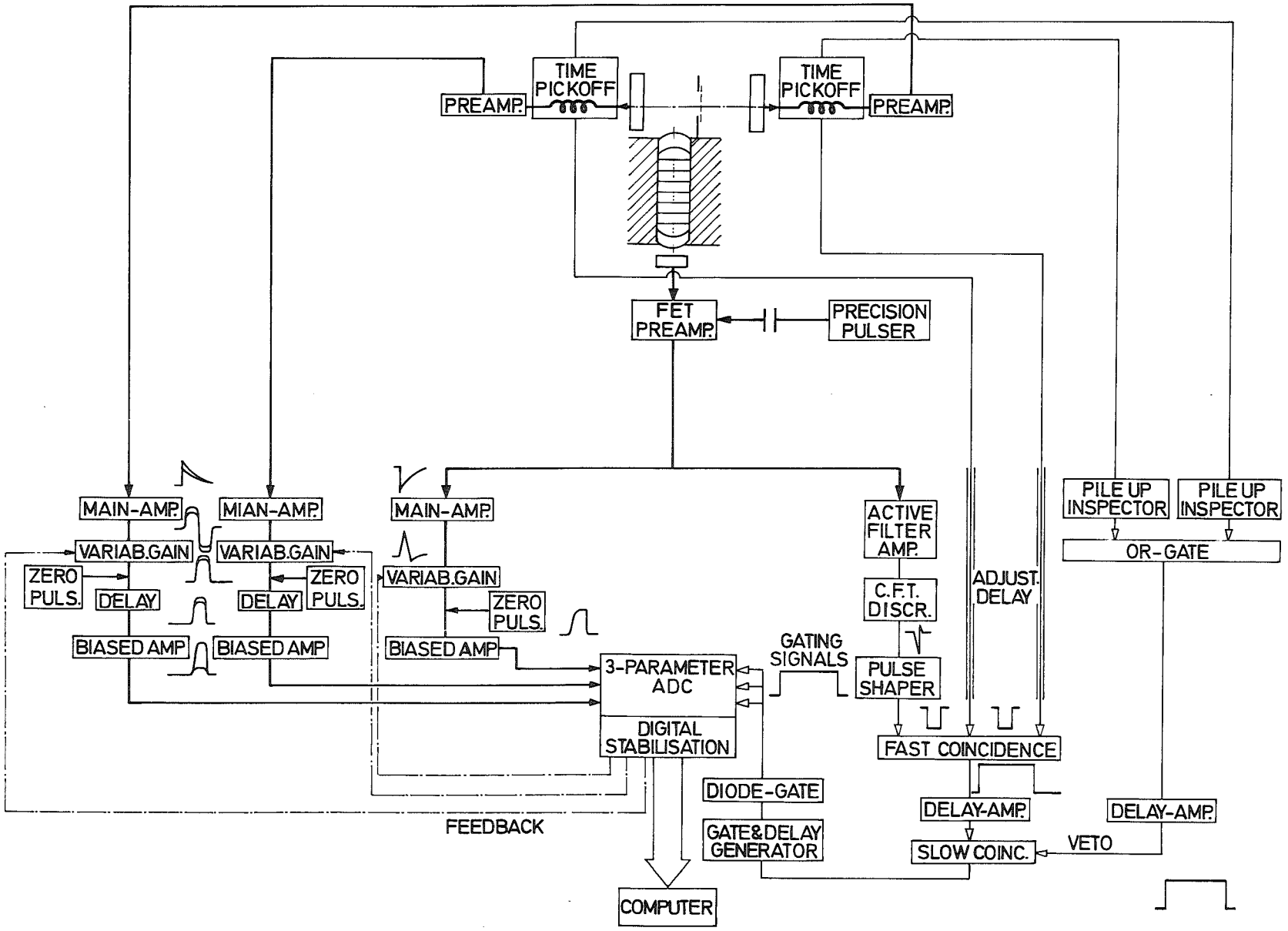
TIME PICKOFF
PREAMP.
TIME PICKOFF
PREAMP.
FET PREAMP.
PRECISION PULSER
MAIN-AMP.
MIAN-AMP.
MAIN-AMP.
ACTIVE FILTER AMP.
PILE UP INSPECTOR
PILE UP INSPECTOR
OR-GATE
VARIAB.GAIN
VARIAB.GAIN
VARIAB.GAIN
ZERO PULS.
DELAY
DELAY
ZERO PULS.
ZERO PULS.
C.F.T. DISCR.
ADJUST. DELAY
BIASED AMP
BIASED AMP
BIASED AMP
GATING SIGNALS
3-PARAMETER ADC
PULSE SHAPER
DIGITAL STABILISATION
FAST COINCIDENCE
DIODE-GATE
DELAY-AMP.
DELAY-AMP.
GATE&DELAY GENERATOR
VETO
SLOW COINC.
FEEDBACK
COMPUTER

Fig. 4

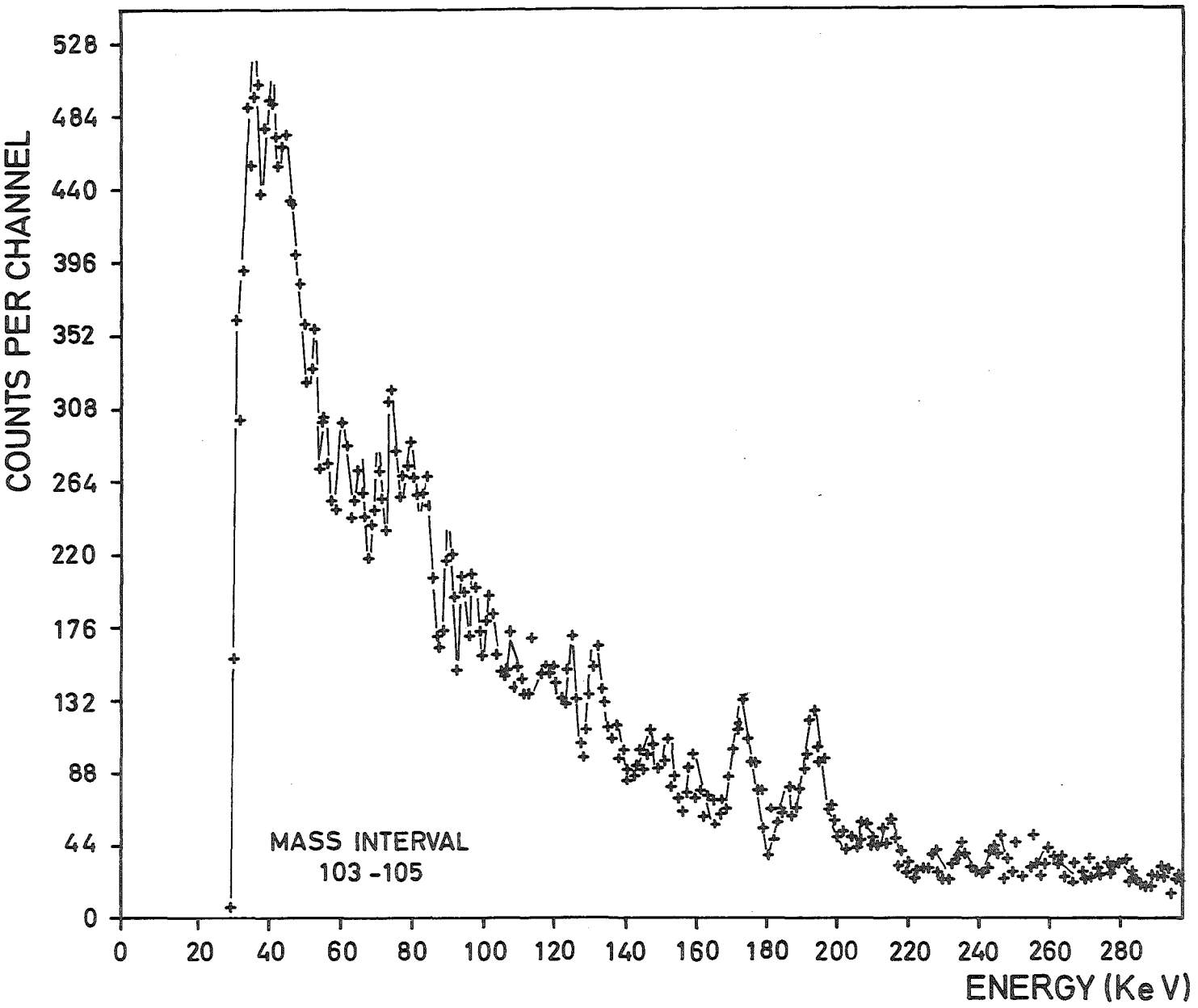
COUNTS PER CHANNEL
528
484
440
396
352
308
264
220
176
132
88
44
0
MASS INTERVAL
103 -105
0
20
40
60
80
100
120
140
160
180
200
220
240
260
280
ENERGY (Ke V)

Fig. 5

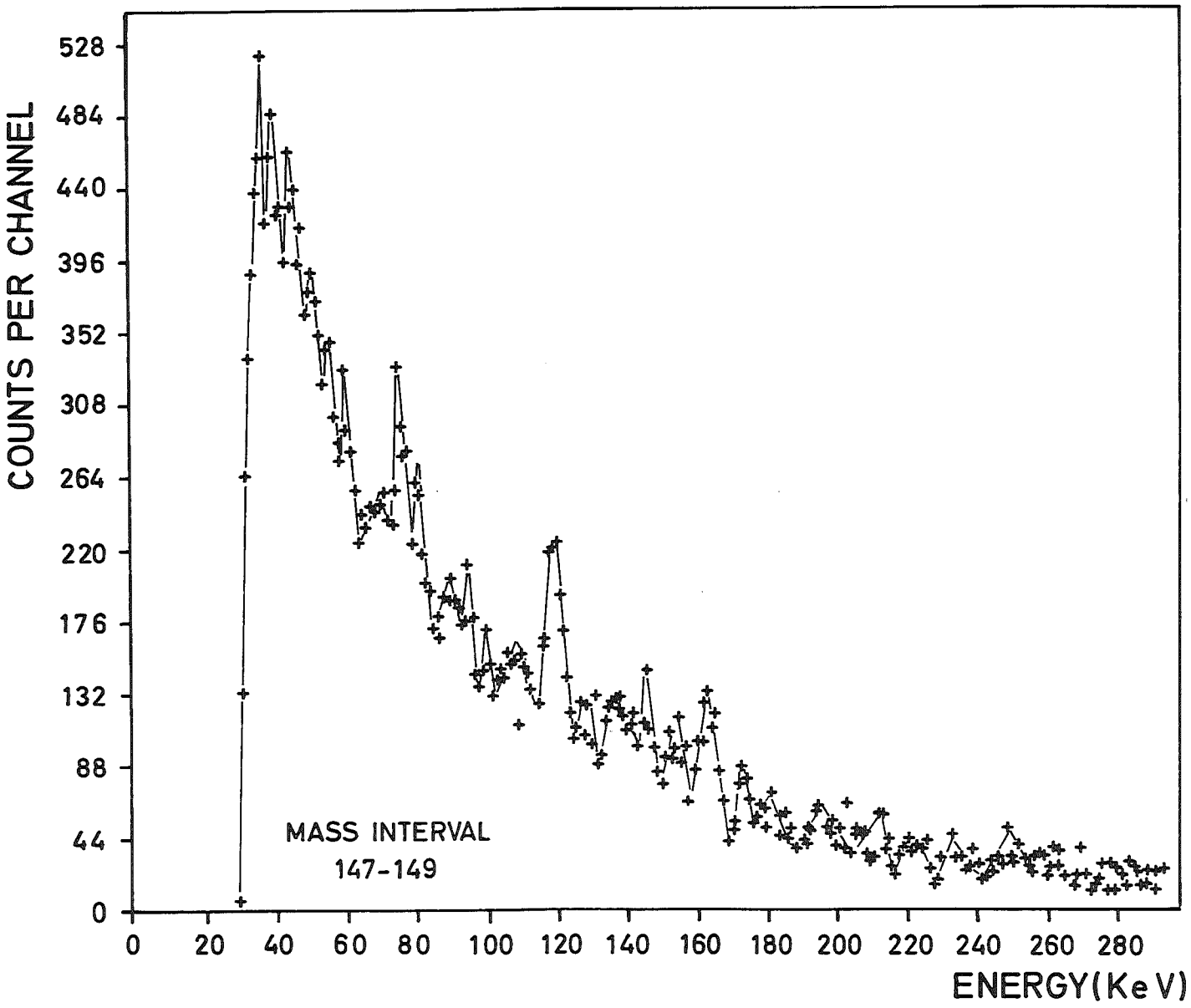
COUNTS PER CHANNEL
528
484
440
396
352
308
264
220
176
132
88
44
0
0
20
40
60
80
100
120
140
160
180
200
220
240
260
280
ENERGY(KeV)
MASS INTERVAL
147-149

Fig. 6

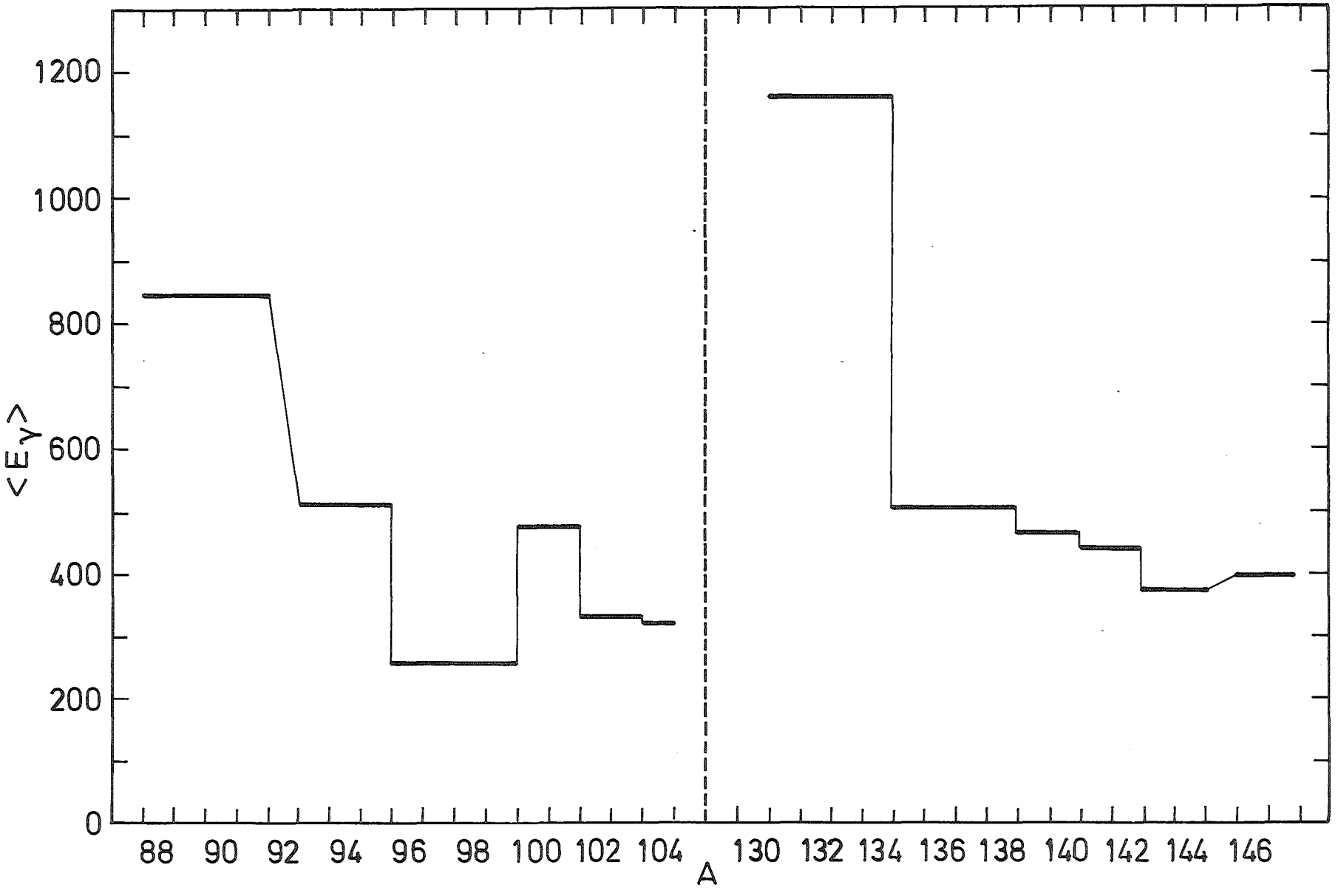
1200
1000
800
600
400
200
0
<Eγ>
88 90 92 94 96 98 100 102 104
130 132 134 136 138 140 142 144 146
A

Fig. 7

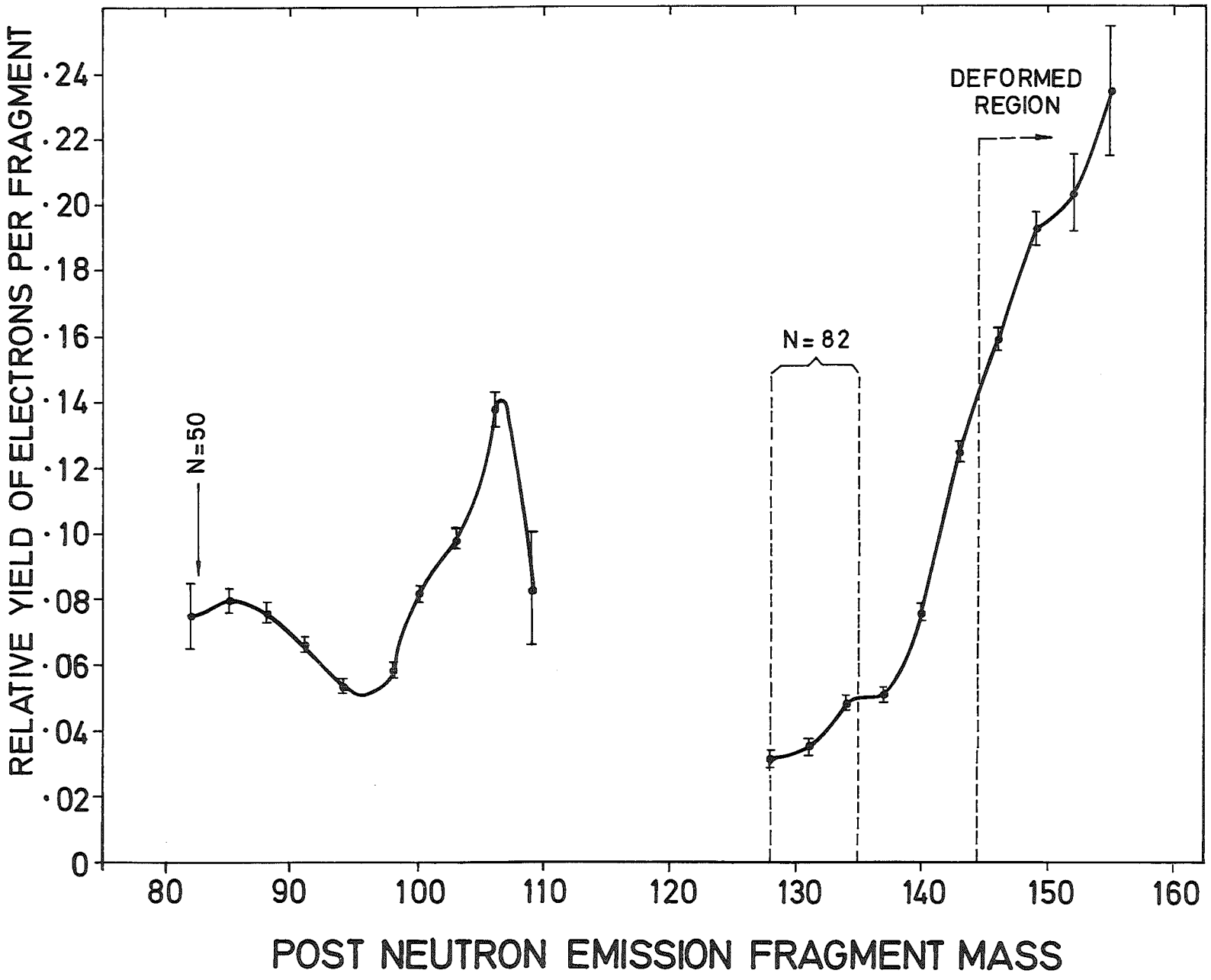
RELATIVE YIELD OF ELECTRONS PER FRAGMENT
·24
·22
·20
·18
·16
·14
·12
·10
·08
·06
·04
·02
0
N=50
N=82
DEFORMED
REGION
80
90
100
110
120
130
140
150
160
POST NEUTRON EMISSION FRAGMENT MASS

Fig. 8

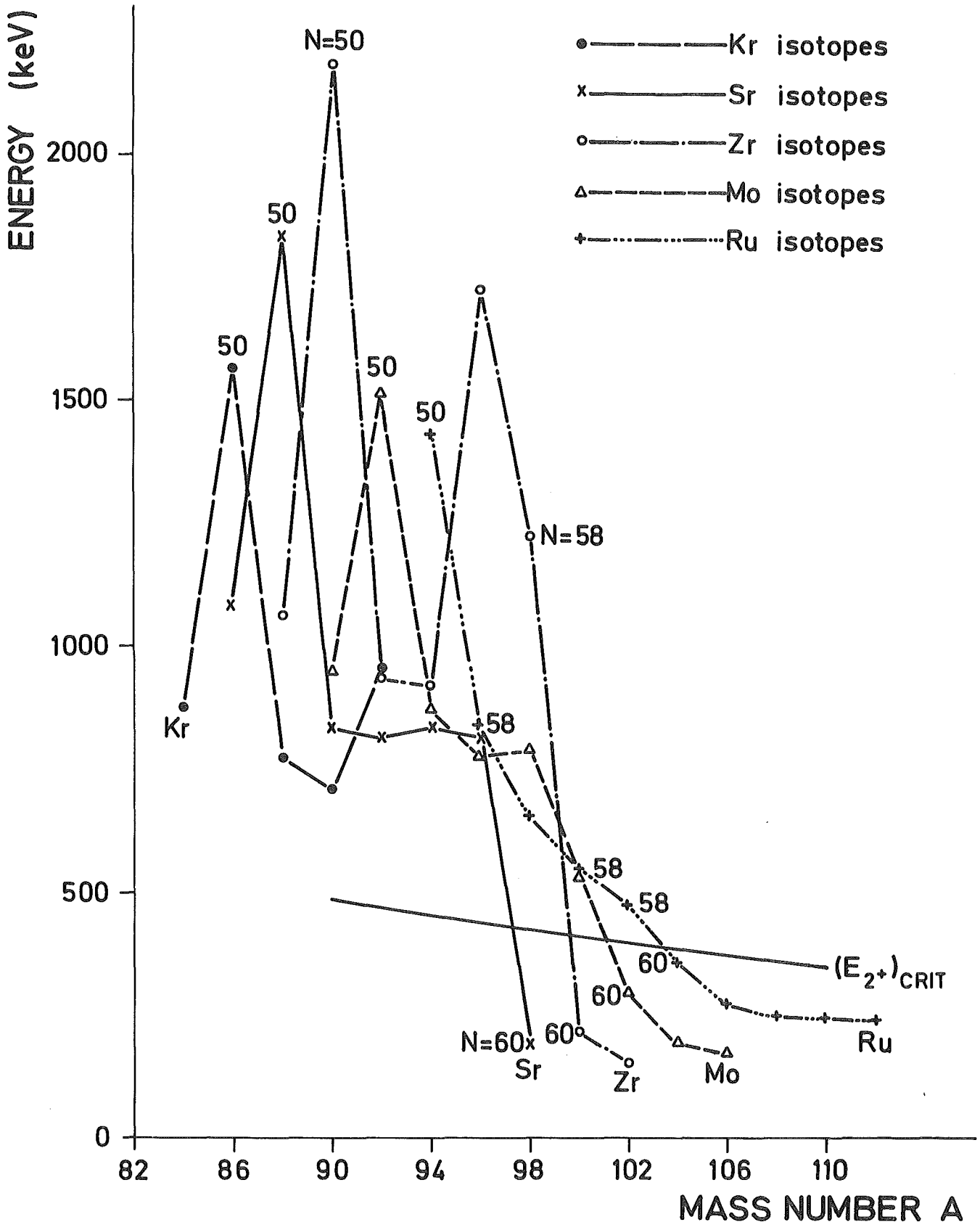
ENERGY (keV)
2000
1500
1000
500
0
82
86
90
94
98
102
106
110
MASS NUMBER A
Kr isotopes
Sr isotopes
Zr isotopes
Mo isotopes
Ru isotopes
N=50
50
50
50
50
N=58
58
58
58
60
60
60
N=60
Kr
Sr
Zr
Mo
Ru
$(E_{2^+})_{CRIT}$

Fig. 9